(Received 8 August 2023, Accepted 13 December 2023, Scheduled 28 December 2023)

Wearable Antenna with Reduced SAR Using Novel FSS Reflector for IoT Assisted Wireless Healthcare Applications

Shivani Sharma* and Malay Ranjan Tripathy

RF and Microwave Lab, Department of Electronics and Communication Engineering
Amity University, Noida 201313, Uttar Pradesh, India

ABSTRACT: In this research work, a flexible polymer-based compact wearable antenna has been designed, fabricated, and analysed for Wireless Body Area Network (WBAN) IoT enabled applications. The antenna is fabricated on a Polyethylene Terephthalate (PET) with λ_L as the lowest operating free-space wavelength resonating for sub-6 GHz band at 2.4 GHz, 3.3 GHz, 4.1 GHz and 5.8 GHz. Periodic Frequency Selective Surface (FSS) reflector is used which reduces Electromagnetic Interference (EMI) antenna and enhances the gain of the antenna. The simulation results prove that this flexible wearable antenna radiates an increased gain of approximately 10 dB and returns loss of -36 dB at the lowest frequency with FSS as a reflector. The simulation results are validated by experimental results which offer a good agreement. An average SAR value of 1.5 watts/gm is measured within the specific safety limit which makes it feasible for practical implementation. This antenna provides better isolation against on-body losses and reduces SAR value with improved radiation efficiency for WBAN IoT enabled applications.

1. INTRODUCTION

The research work in the field of Internet of Things (IoT) is helping to provide efficient solutions in the field of Wireless Body Area Network (WBAN). The effective utilization of wearable devices is vital for on- or off-body communication in WBAN which is possible due to technological advancements in IoT. The principal aim of IoT in WBAN is to combine the electronic equipment with fabric for improved wireless communication and remote sensing [1]. The advancements as well as miniaturization of wearable devices have led to remarkable expansion of WBAN applications. From several applications, for instance, sports, fitness, smart suits, tracking an enemy in military, personal security, and entertainment via wireless devices [2–7], biomedical health-care applications require the foremost utilization of wearable devices in real-time applications by many researchers using various wearable materials and bands [8]. Antenna plays an extremely major role for wearable devices in WBAN as it is responsible for creating the wireless communication link between the internal components as well as external components. The design obligations for the wearable antenna by Federal Communication Commission (FCC) is more distinctive than traditional antennas [9] for Body Centric Communication (BCC). Several research works have been reported in literature review [10–12], but only a few of them focused on the implications of wearable devices on IoT based WBAN technology. The work on reconfigurability structure has been recently explored by various researchers [13, 14] and focused on low-capacitance, low-power consumption diodes to digitally control the modification of the radiation pattern making it reconfigurable [15, 16], but due to active components, the antenna structure may not be practically effective when being used in WBAN. Similar to the above work, Haydhah et al. [17] presented a reconfigurable antenna using P-I-N diode with two modes to switch with the total radiated gain of 1.6 dB only. Numerous issues can be raised due to on-body RF coupling affecting the performance of wearable devices [18–20]. Electro-magnetic (EM) radiation has a damaging impact on the human tissues; therefore, radiation level must adhere to the Specific Absorption Rate (SAR) level. The resonance frequency of the designed antenna also gets affected by the human on-body losses. After considering all the challenges that can affect the wearable antenna performance in a complex environment, the wearable substrate material must be carefully chosen [18]. The substrate material used for wearable antennas must be high heat resistant, highly absorptive, and flexible [21, 22] which has been discussed in a research article on a low SAR wearable antenna. The physical constraints include some other requirements such as low SAR level, miniaturized structure, compactness, flexibility, low power dissipation, high bending capabilities, low loss tangent, and low dielectric value [23, 24].

The substrate material has a major impact on the human body and on the characteristic properties of radiating patch. Therefore, various polymer-based materials with a lower value of dielectric constant (ε_r) and low loss tangent ($\tan\delta$) are ideally preferred since they make antenna less lossy, and better radiation efficiency is achieved [25–27]. Here, a periodically arranged FSS reflector is used between the radiating patch and human body to reduce radio frequency (RF) coupling thus providing better isolation by lowering the SAR value [28, 29] which increases the radiation efficiency. Numerous researchers have recently explored IoT based WBAN which is power efficient, utilizes wide bandwidth, has better radiating gain, has reduced SAR, has less interference, and has practically low profile. In

* Corresponding author: Shivani Sharma (shivaniaeri25@gmail.com).

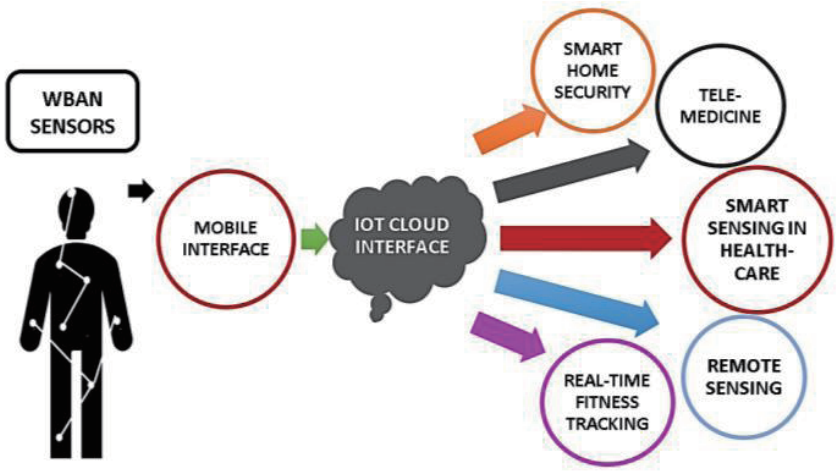

FIGURE 1. IoT scenario in WBAN for real-time smart sensing.

the work by Hussain [30], IoT antenna for multi-band have been published 6 GHz band and mm-wave spectrum covering 27.4–28.4 GHz. The use of IoT in wireless communication has resulted in a substantial increase in power consumption. The research work on energy efficiency (EE) based on a simultaneous wireless information and power transfer (SWIPT) distributed antenna system by splitting and adjusting the power of distributed antenna ports is presented by Huang et al. [31, 32].

This paper is organized in the following sections, i.e., Section 1 describes the background study; Section 2 includes the design and configuration; Section 3 covers the simulated and experimental results, and the final Section 4 concludes the findings of this research work.

1.1. IoT Technology in Wireless Body Area Network

The wireless communication for WBAN applications is more complicated than traditional wireless networks. There remain a few major challenges to establish a stable communication link for wearable devices in Industrial, Scientific, and Medical (ISM) bands due to its license free nature. The technical advancements and device size reduction of wireless devices have led to tremendous growth for WBAN applications using IoT [33–35]. The primary purpose of IoT technology in WBAN is to merge electronic equipment with a flexible device for real-time automatic sensing. The physical constraint includes some requirements for safety regulations, such as low SAR level, low power dissipation, low EMI, low loss tangent, and low dielectric value [36, 37]. The use of IoT is making real-time tracking easier for various WBAN applications such as telemedicine, biomedical sensing, smart sensing in healthcare, smart parking, automatic fitness tracking, and remote monitoring. Davoli et al. [38] carried out the research work at University of Parma, Italy and developed a progressive method for merging short-range IoT networks called micro IoT, with more contemporary long-range LPWANs called macro IoT. A smart IoT based intelligent parking system using dual lens antenna is analyzed and implemented by Cai et al. [39].

IoT and WBAN when being merged can lead to major advancement in technology, shown in real-time scenario given above in Fig. 1.

1.2. FSS Backed Reflector Antenna Patch for High Gain

In this work, a wearable flexible antenna is designed along with the flexible FSS sheet below the antenna as an FSS reflector to improve the gain and reduce the on-body proximity losses. This arrangement of FSS sheets can be used along with the antenna to reduce the on-body loss with zero phase reflection [4, 5]. The FSS sheet is designed using babinet's principle and considering grating lobe criterion which is finally positioned below the antenna forming an FSS reflector to increase the radiation efficiency as well as gain. A Defective Ground Structure (DGS) plane with an FSS reflector [40, 41] to get multi-band frequency response is used. This antenna structure has reduced SAR value and RF coupling between the device and human tissue.

1.3. Fundamental Principle

The basic principle for FSS spectral domain analysis can be explained using Floquet's port principle which states that when an incident wave illuminates on an infinite, periodic, planar sheet, each unit cell on an array of periodic structure must generate equal current and electric field. The in-band waves are transmitted in phase with that of incident wave, and out-band waves are reflected back. Fig. 2 clearly demonstrates the principle of operation of FSS reflector.

2. CONFIGURATION OF THE PROPOSED ANTENNA

2.1. Proposed Polymer-Based Flexible Antenna

For the fabrication of proposed antenna, a flexible polymer-based substrate material Polyethylene Terephthalate (PET) is used due to its low cost and easily moldable structure in different shapes. The low dielectric constant of 2.25 and low loss tangent of 0.001 make it the best choice for low-microwave frequency wearable applications. The substrate's dimensions are Sx (width) by Sy (length) with the thickness (t) of 2 mm with

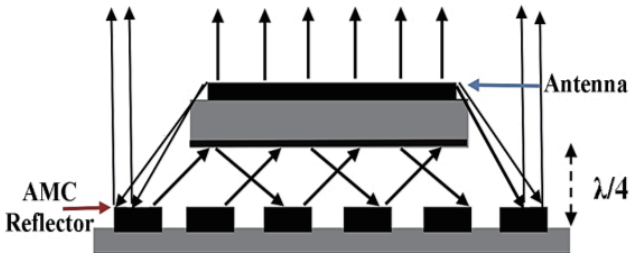

FIGURE 2. Proposed antenna arrangement with FSS reflector.

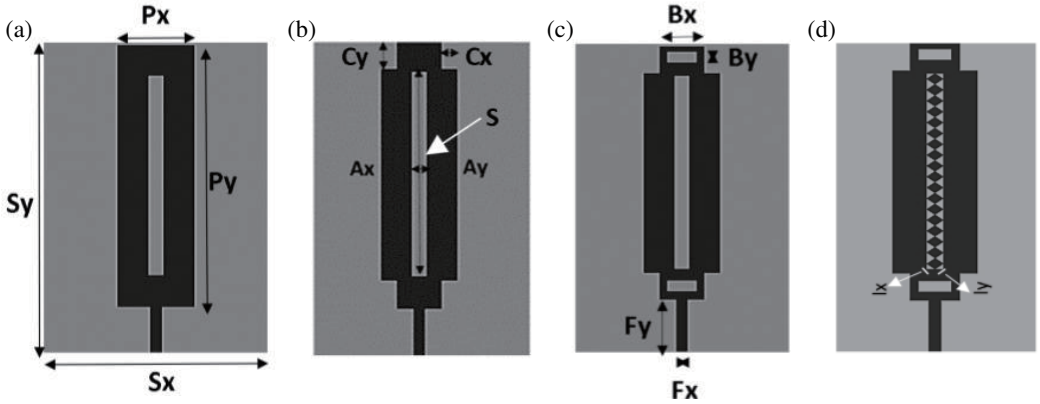

FIGURE 3. Iteration process of the proposed wearable patch. (a) Iteration 0, (b) Iteration 1, (c) Iteration 2 and (d) Final antenna geometry.

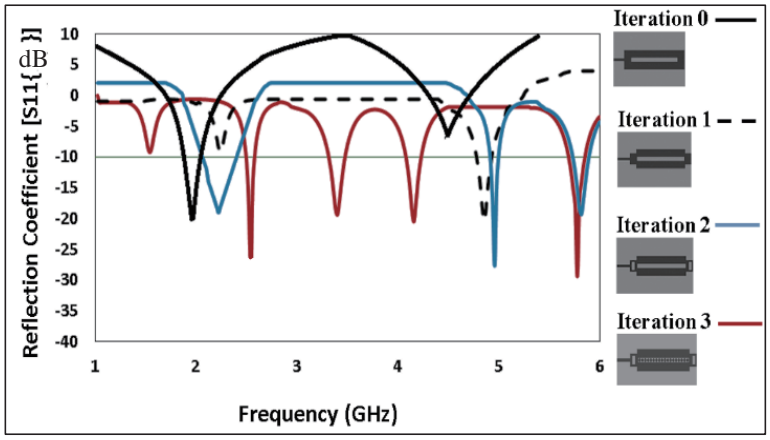

FIGURE 4. Reflection coefficient of all the iterative structures.

similar dimensions for ground plane. A rectangular conductive patch is etched with overall dimensions of Px (width) by Py (length). The iteration process of the conducting copper patch is given in Fig. 3. The steps for evolution process of the finalized antenna are given below:

Step 1: The center slot is sliced out from the patch of length A_X and width A_Y in Iteration 0 [refer Table 1 and Fig. 1(a)].

Step 2: In Iteration 1, two side slots having length B_X and B_Y are sliced out from the initial and end points of the patch.

Step 3: In Iteration 2, four corner slots having equal length C_X, and C_Y are sliced out from the edges.

The geometrical description calculated using the microstrip transmission line theory [42] is given in Table 1.

The iterative patch structures are processed and analyzed at every stage which is compared in terms of reflection coefficient v/s frequency response for required bandwidth (refer Fig. 4).

2.2. Proposed Polymer-Based Flexible Antenna with FSS Reflector

For the fabrication of FSS reflector, the same flexible polymer-based substrate material PET is used. The geometrical parameters of periodic structure on FSS reflector are calculated using

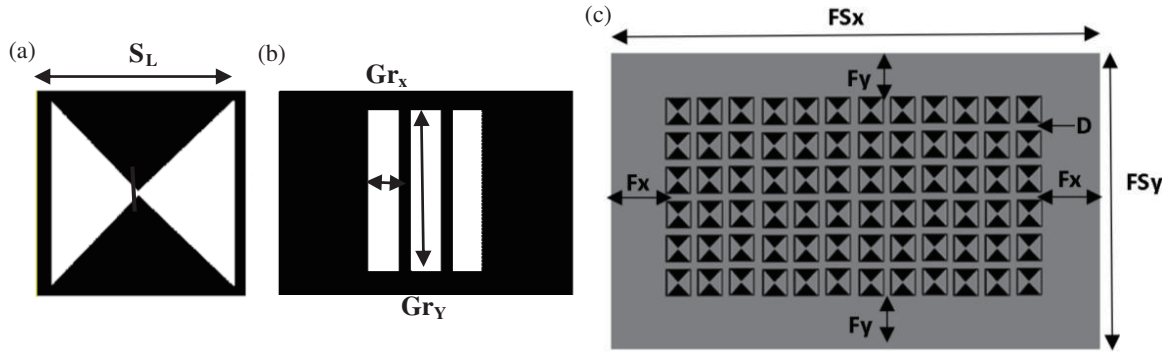

FIGURE 5. (a) Unit cell of FSS Reflector sheet. (b) DGS sheet below reflector. (c) 6 by 12 array structure over FSS reflector.

TABLE 1. Geometrical description: proposed polymer-based antenna.

PARAMETERS	VALUE
Sx, Sy	$59 * 133\,\text{mm}^2$
Px, Py	$20 * 95\,\text{mm}^2$
Ax, Ay	$4 * 72\,\text{mm}^2$
Bx, By	$5 * 10\,\text{mm}^2$
Cx, Cy	$4 * 8\,\text{mm}^2$
$Ix = Iy$	$2 * 2\,\text{mm}^2$
Fx, Fy	$3 * 19.5\,\text{mm}^2$
S	4 mm

TABLE 2. Geometrical description: proposed FSS reflector.

PARAMETERS	VALUE
Fs_X, Fs_Y	$104.5 * 143.5\,\text{mm}^2$
S_L	8 mm
D	2.5 mm
F_X, F_Y	$10 * 10\,\text{mm}^2$
Gr_X, Gr_Y	$10 * 20\,\text{mm}^2$

the theory of Floquet's port and analyzed by Method of Moment spectral [43]. Table 2 shows all the dimensions of metamaterial array.

The unit cell of the proposed FSS based periodic structure and 6 by 12 array is finally etched over the substrate [refer Fig. 5(a)]. The arrangement of DGS ground sheet below FSS reflector is shown in Fig. 5(b). The substrate is sandwiched between the reflective FSS array patch and the DGS plane shown in Fig. 5(c). The design parameters of FSS unit cell (a, S_L and D) can be calculated using given equations [43]:

$$\text{Periodicity} = k\frac{c}{2fpass\sqrt{\varepsilon r}}\cos\left[\arcsin\left(\frac{1}{\sqrt{\varepsilon r}}\sin\theta\right)\right] \quad (1)$$

$$\text{Overall array length } (a) \approx \lambda_L/3 \quad (2)$$

$$\text{Length of the unit cell } (S_L);\ \frac{\lambda_L}{25} \leq S_L \leq \frac{\lambda_L}{15} \quad (3)$$

Onset grating lobe condition is important since it can lead to out of phase wave transmission of higher order Floquet's waves in space. This condition relies on the incident wave angle and on the inter-element spacing (D) given below:

$$D = \frac{\lambda_g \times n}{(\sin\eta + \sin\eta g)} \quad (4)$$

$$\lambda_g = \frac{c}{f_g} \quad (5)$$

λ_g is the guided wavelength, c the speed of light, and n the number of elements. When the incident wave is perpendicular, i.e., $\eta_g = 90°$, the inter-element spacing becomes:

$$D = \frac{\lambda_g \times n}{(\sin\eta + 1)} \quad (6)$$

$$\text{In general terms, } D \text{ must be } \leq 0.5\lambda_L \quad (7)$$

3. ANALYTICAL MODELLING OF THE PROPOSED ANTENNA

In this section, the performance of the proposed wearable antenna is analyzed and examined on the basis of various aspects and properties by means of ECM, SAR analysis, bending analysis, and power analysis.

3.1. Equivalent Circuit Modelling of Proposed Antenna with FSS

The ECM for the proposed antenna based on the transmission line theory is shown for each slot individually given below [refer Fig. 6] and is explained in following steps:

Step 1: The equivalent circuit of the center slot has been considered in which the inductor and capacitor are in parallel resonance with an antenna.

Step 2: Similarly, Lc_1, Lc_2, Lc_3, Lc_4 and Cc_1, Cc_2, Cc_3, Cc_4 represent the equivalent inductances and capacitances of

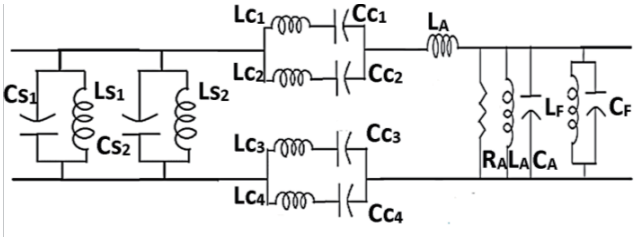

FIGURE 6. ECM of proposed slotted wearable patch antenna.

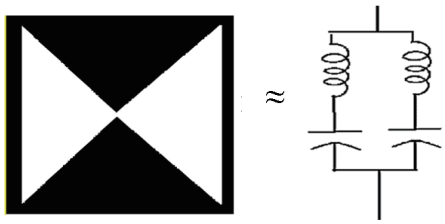

FIGURE 7. ECM of unit cell of proposed FSS reflector.

four corner slots on the patch, and the periodic structure's overall inductance is Lp_1.

Step 3: Now, Ls_1, Ls_2 and Cs_1, Cs_2 are parallelly connected to overall circuit in series resonance.

The topology of overall equivalent circuit model of the proposed wearable antenna for resonance model based on R, L, C networks is shown in which one center slot with a periodic structure, two side slots, four corner slots are added to the elementary RLC model representing microstrip feed line whose inductance and capacitance are L_F and C_F, respectively [45, 46]. The unit cell showing square ring loop with hourglass shaped slots can be represented by a simple series-shunt RLC resonant circuit (refer to Figure 7) in following steps:

Step 4: The inductance is generated due to square metallic loop ring L_S, and the gap between the unit cells represents the capacitance C_g.

Step 5: Similarly, inner hourglass slots are represented by the capacitance C_i, and the metallic shape represents the inductance, L_i. Overall inductance and capacitance can be modified by modifying gap between the unit cells' inter-element spacing (D), overall length of the array (a), and thickness (t) of the metallic layer. The overall inductance and capacitance are given in following equations:

$$Cg \approx \varepsilon r \varepsilon o \frac{(a \times t)}{D} \tag{8}$$

where $\varepsilon_o = 8.85 \times 10^{-12}$ f/m, t = thickness of the metallic patch

$$Cs \approx \varepsilon r \varepsilon o \times t \tag{9}$$

Therefore, total C_T can be calculated using Equation (9) :

$$C_T \approx \varepsilon r \varepsilon o \times t \frac{(a+D)}{D} \tag{10}$$

Now, the series inductance of unit cell and total array inductance are given by:

$$Ls \approx 2a \left[\log \frac{2a}{t} + \frac{1}{2}\right] \tag{11}$$

$$\text{and } L_T = \frac{L_S}{6} \tag{12}$$

$$\text{Therefore, } L_T = \frac{a}{3}\left[\log \frac{2a}{t} + \frac{1}{2}\right] \tag{13}$$

Since transmission line total impedance is in series with static capacitance C_0, the bandwidth of the proposed structure can be calculated using Equation (17):

$$B_T = \frac{R}{L_T C_T} \tag{14}$$

At lower frequencies, capacitance dominates the overall effect on the input impedance of the antenna, and at higher frequencies, inductance dominates. The equivalent impedances for both the cases are given below:

$$Z_{eq}(f_L) = \frac{1}{2\pi f C_{0,0}} \tag{15}$$

$$Z_{eq}(f_H) = 2\pi f j L \tag{16}$$

where $C_{0,0}$ is the coverall capacitance at lower frequencies, and L is the overall inductance at higher frequencies.

3.2. Floquet's Port Analysis

The analysis of proposed FSS sheet reflector is performed using Floquet's port analysis, and the reflection coefficient is plotted against the required range of frequencies in Fig. 8.

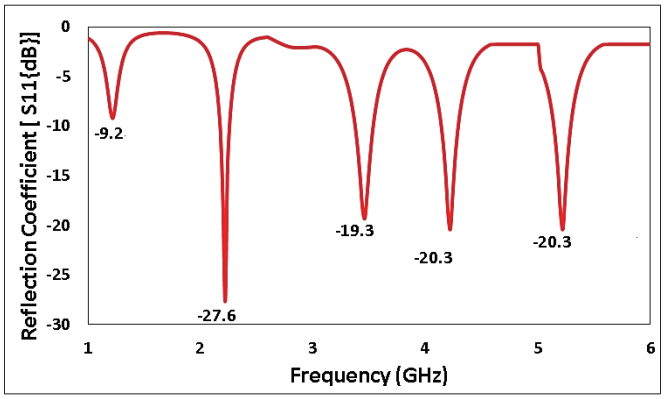

FIGURE 8. Reflection coefficient of proposed FSS sheet only.

3.3. SAR Analysis

The designed wearable antenna can be detuned owing to the absorption of large amount of radiated power by human body, and thus gain of the antenna is mostly reduced. Hence, the bending conditions and SAR analysis are studied for on-body wireless communications [44]. SAR is the maximum value of EM radiation emitted by any wireless device which can be absorbed by

biological tissue. The greater value of SAR than this can possibly injure the tissue cells gradually. The value of constant (ε_r), conductivity (σ), mass density (D), and thickness (T) must be considered before designing the antenna for wireless wearable communication in WBAN shown in Fig. 9 [32].

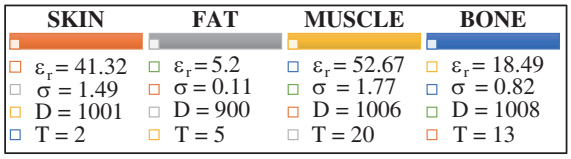

FIGURE 9. Human tissue layer's properties for SAR analysis.

To keep the antenna within the safer limit, the Federal Communication Commission (FCC) has set some specific SAR values of less than or equal to 1.6 Watt/kg over 1 g of tissue, and it is usually measured over 1 gram, or 10 grams of tissue weight and given in the following equations:

$$\text{SAR} = \frac{\sigma}{\rho} E_{rms}^2 = \frac{1}{V} \int \frac{\sigma(r) |E(r)|^2}{\rho(r)} dr \tag{17}$$

where V is the volume of the sample, E the mean RMS value of the electric field (V/m), σ the conductivity (S/m), and ρ the density of the tissue (Kg/m^3).

The IEEE's standard for SAR is equivalent to 2 watts/kg over 10 g of tissue according to section C95.1-2005 [44]. This value is also recognized by International. Commission on Non-Ionizing Radiation Protection (ICNIRP). The amount of EM radiation absorbed may lead to a change in the temperature of tissue and is given by:

$$\text{SAR}(\Delta T) = C(\Delta T) \tag{18}$$

where (ΔT) is the duration of exposure, and C is the discharged heat.

To validate the performance of the proposed antenna for wearable applications, the antenna must be studied under different bending conditions at different angles. The SAR field is within the safety limit, and the surface charge is also negligible as shown in Fig. 10. To overcome this, the antenna must

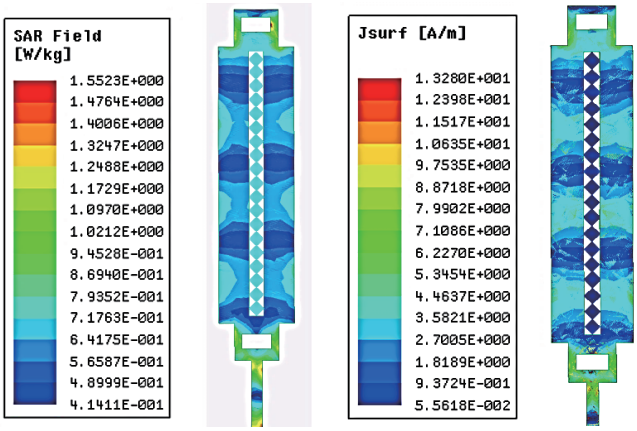

FIGURE 10. SAR value evaluation under bending condition with Surface charge.

have a wider range of frequency, and also FSS reflector helps the antenna to maintain a stable response for required range.

3.4. Power Consumption Analysis

After multiple reflections occur inside the cavity for gain enhancement at the first resonance condition, the maximum power reflected is given by the following equation:

$$P(\theta)_{max} = \frac{1 - R^2(\theta)}{1 + R^2(\theta)} P(\theta)_{min} \tag{19}$$

$P(\theta)_{\text{min}}$ is the radiation pattern of the antenna at minimum boresight angle, i.e., $\theta = 0$ where $R(\theta)$ is the complex conjugate of the reflection coefficient S_{11}, and θ is the boresight angle at which reflection occurs. The received power can be given using Friss's equation as follows:

$$P_{RX} = P_{TX} + G_{TX} - P_{cl} - F_{SL} - L_{ATT} P(\theta)_{\text{max}} \tag{20}$$

Considering zero sensitivity of RFID tag hence making P_{RX} to be negligible, the attenuation can be calculated based on this assumption, and the equation becomes:

$$P_{att} = P_{TX} + G_{TX} - P_{cl} - F_{SL} \tag{21}$$

$$P_{att} = 30 + 10 - 3 - 32.75 \tag{22}$$

This covers approximately all the RFID tags in the market. The Off set should be applied only when there is a requirement for application.

P_{Tx} is the transmitted power (ranges between 10 to 33 dBm); P_{Rx} is the received power; P_{cl} is the cables loss (generally 3 dB); G_{Tx} is the transmitted gain; L_{ATT} is the overall attenuation loss due to various factors; F_{SL} is the free space loss (32.75 dB/m). The attenuation in the transmission is calculated using given Eq. (28):

$$P_{att} = 4.25 \text{ dBm} \tag{23}$$

The transmitted power by the reader is calculated using the above equations and according to FCC guidelines is given below:

$$P_{RX} = 30 - 4.25 = 25.75 \approx 26 \text{ dBm} \tag{24}$$

4. SIMULATED AND EXPERIMENTAL RESULTS OF PROPOSED FSS BACKED ANTENNA STRUCTURE

The analysis and simulation of the proposed designed antenna are done using ANSYS High Frequency Structure Simulator (HFSS) version 19.

4.1. Return Loss for Impedance Matching

The microstrip feedline with normalized 50 Ω impedance is used as RF feed. The simulated values of S_{11} are −36 dB at 2.4 GHz, −25 dB at 3.3 GHz, −20 dB at 4.1 GHz, and −30 dB at 5.8 GHz, respectively, as shown in Fig. 11.

4.2. Radiated Gain and Radiation Efficiency

The measured value of gain is equivalent to 5 dB at the lowest frequency which is incremented to 10 dB FSS reflector. The back radiation is also reduced due to FSS reflector.

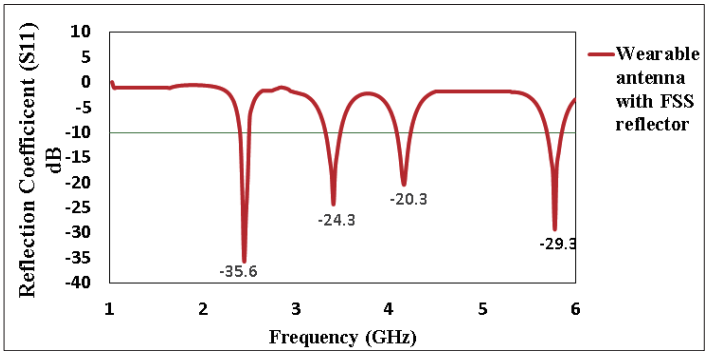

FIGURE 11. Reflection coefficient of antenna with FSS reflector.

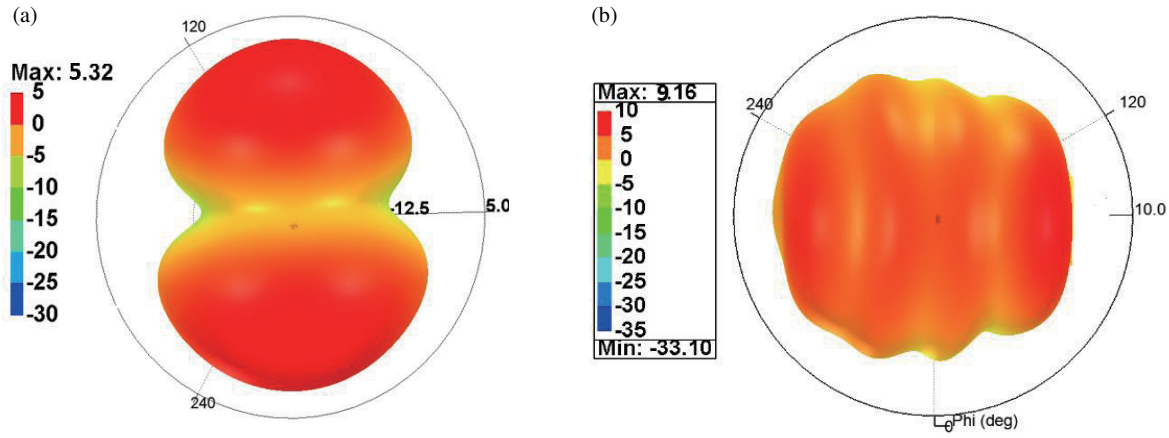

FIGURE 12. 3D plot for the gain of the presented antenna (a) without and (b) with the FSS reflector.

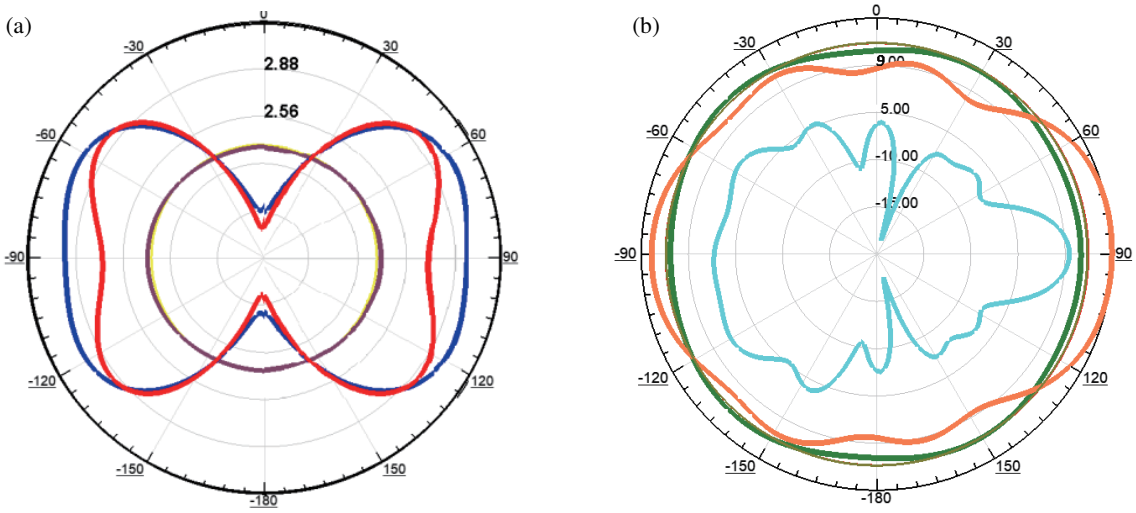

FIGURE 13. (a) Radiation efficiency of antenna $\varphi = 0°$, $90°$, $180°$ and $360°$ with constant $\theta = 0$ (a) without FSS, (b) with FSS.

The 3D radiation graph against frequency is plotted and shown in Fig. 12. The radiation efficiency at different values of φ, i.e., $0°$, $90°$, $180°$, $360°$ keeping θ constant is shown in Fig. 13 where θ and φ are analyzed for horizontal and vertical antenna polarizations, respectively. Various strategies such as periodic patch, partial slotting, FSS Reflector, DGS are used to achieve a selective isolated response at multi-frequency covering the ISM bands for in-band transmission and out-band rejection with increased radiated gain.

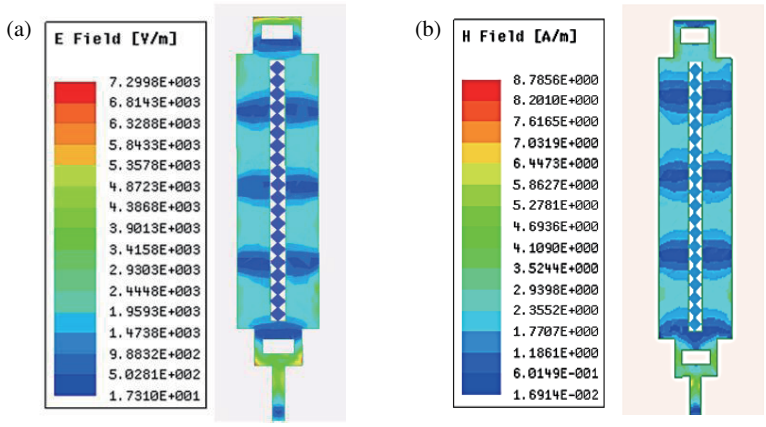

FIGURE 14. (a) Electric filed distribution. (b) Magnetic field distribution.

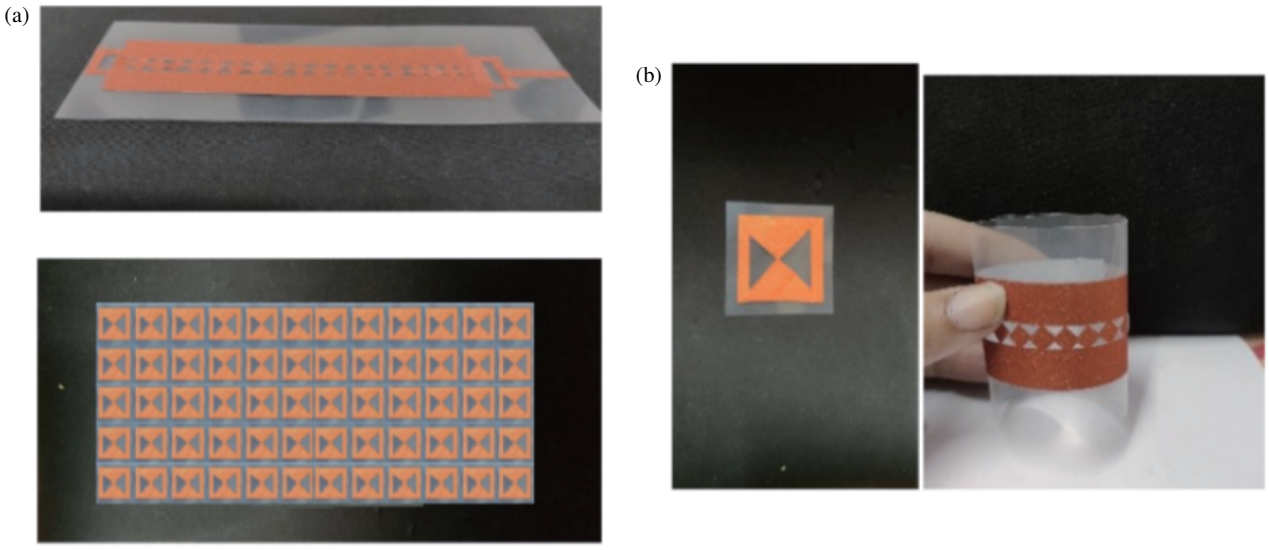

FIGURE 15. Arrangement of fabricated, (a) proposed wearable antenna, (b) proposed FSS reflector array.

TABLE 3. Comparison of previous work with this proposed research work.

Ref. No.	Freq. band	Substrate	Return Loss (dB)	Max. Gain (dB)	SAR (watts/kg) for 10 gm of tissue
[31]	2.45, 3.65	Denim	−25	7.35	1.25
[32]	4.9, 5	Nylon	−15.2	6.7	Not calculated
[33]	2.4	Duroid 5880	−19	2.6	1.58
[34]	2.4,5.8	Duroid 5880	−21	3.5	1.6
This work	2.4, 3.3, 4.2, 5.8	Polymer (PET)	−36, −25, −20, −30	10	1.5

4.3. Current Distribution

Figure 14 shows the electric and magnetic fields on the antenna's radiating patch element. It is evident in the given figure that E and H fields are equally distributed from center slot to the edges.

The proposed antenna structure is fabricated, and the experimental results are measured using Vector Network Analyzer (VNA). All the simulated results are validated by experimental ones in Fig. 15.

The total realised gain v/s resonant frequency of fabricated antenna at constant values of θ and φ is measured. It is noticeable that the gain is maximum at 2.4 GHz when FSS reflector is placed at a distance of 6 mm from radiating antenna. The simulated results are validated by experimental ones which shows a good agreement between simulated and measured values [refer to Figs. 16(a), (b)].

The presented work is justified in Table 3, which comprises a brief comparison between this research and available research work in the same applicable field. This antenna radiates for

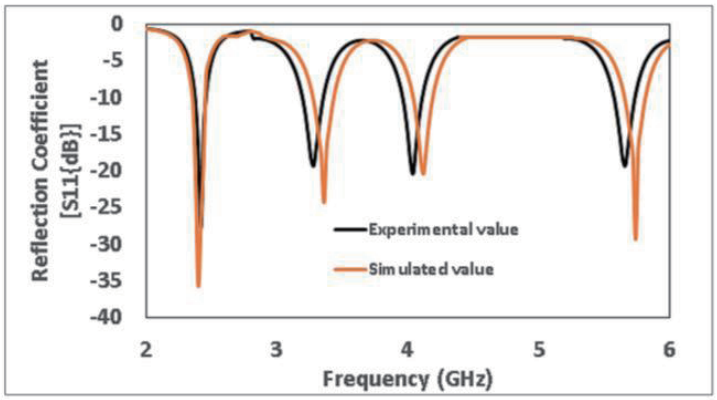

FIGURE 16. Experimentally validated result of fabricated antenna.

complete sub-GHz band at multiple resonant frequencies which are 2.4, 3.3, 4.2, 5.8. It is made up of polymer based material, i.e., PET, which is excellent for wearable applications with minimal cost for fabrication. The measured results are compared in Table 3 which shows that the antenna impedance matching is good as return loss achieved is good compared to other work. The most important factor to be considered for WBAN applications is SAR value which in this case is achieved to be 1.5 watt/10 gm of the tissue. The SAR value achieved for this wearable antenna is within the specified value with advantage of maximum gain of 10 dB due to FSS reflector used which compared with previous work can be noticed in terms of radiated gain.

5. CONCLUSION

A compact polymer-based flexible wearable antenna with an FSS reflector has been designed and analyzed for Wireless Body Area Network. The antenna operates for sub-6 GHz band i.e., 2 GHz to 6 GHz with periodic radiating patch. A DGS ground plane is used to get multi-band response along with flexible FSS reflector below to provide better isolation between the body and the patch. This approach reduced RF coupling which lowered the SAR value to 1.5 watts/gm to meet the safety limit. The wearable antenna with FSS reflector exhibits a very high gain with good radiation efficiency in all directions. The antenna structure is miniaturized by partial slotting, and PET flexible substrate is used to make it compact for wearable applications in WBAN.

ACKNOWLEDGEMENT

This research article is dedicated to my guide, Late Dr. M. R. Tripathy, who was my biggest source of motivation in this research field.

REFERENCES

[1] Ademaj, F., M. Rzymowski, H.-P. Bernhard, K. Nyka, and L. Kulas, "Relay-aided wireless sensor network discovery algorithm for dense industrial IoT utilizing ESPAR antennas," *IEEE Internet of Things Journal*, Vol. 8, No. 22, 16 653–16 665, Nov. 2021.

[2] Ashyap, A. Y. I., S. H. B. Dahlan, Z. Z. Abidin, M. I. Abbasi, M. R. Kamarudin, H. A. Majid, M. H. Dahri, M. H. Jamaluddin, and A. Alomainy, "An overview of electromagnetic band-gap integrated wearable antennas," *IEEE Access*, Vol. 8, 7641–7658, 2020.

[3] Paracha, K. N., S. K. A. Rahim, P. J. Soh, and M. Khalily, "Wearable antennas: A review of materials, structures, and innovative features for autonomous communication and sensing," *IEEE Access*, Vol. 7, 56 694–56 712, 2019.

[4] Zhao, B., J. Mao, J. Zhao, H. Yang, and Y. Lian, "The role and challenges of body channel communication in wearable flexible electronics," *IEEE Transactions on Biomedical Circuits and Systems*, Vol. 14, No. 2, 283–296, Apr. 2020.

[5] Wong, H., W. Lin, L. Huitema, and E. Arnaud, "Multi-polarization reconfigurable antenna for wireless biomedical system," *IEEE Transactions on Biomedical Circuits and Systems*, Vol. 11, No. 3, 652–660, Jun. 2017.

[6] Belrhiti, L., F. Riouch, A. Tribak, J. Terhzaz, and A. M. Sanchez, "Flexible antennas design and test for human body applications scenarios," *Microwaves, Optoelectron. Electromagn. Appl.*, Vol. 16, No. 2, 494513, 2017.

[7] Kim, J., A. S. Campbell, B. E.-F. De Avila, and J. Wang, "Wearable biosensors for healthcare monitoring," *Nature Biotechnology*, Vol. 37, No. 4, 389–406, Apr. 2019.

[8] Dey, S., M. S. Arefin, and N. C. Karmakar, "Design and experimental analysis of a novel compact and flexible super wide band antenna for 5G," *IEEE Access*, Vol. 9, 46 698–46 708, 2021.

[9] Commission, F. C., "FCC report and order for part 15 acceptance of ultra wideband (UWB) systems from 3.1-10.6 GHz," *FCC, Washington, Dc*, 1–10, 2002.

[10] Saeed, S. M., C. A. Balanis, C. R. Birtcher, A. C. Durgun, and H. N. Shaman, "Wearable flexible reconfigurable antenna integrated with artificial magnetic conductor," *IEEE Antennas and Wireless Propagation Letters*, Vol. 16, 2396–2399, 2017.

[11] Wong, H., W. Lin, L. Huitema, and E. Arnaud, "Multi-polarization reconfigurable antenna for wireless biomedical system," *IEEE Transactions on Biomedical Circuits and Systems*, Vol. 11, No. 3, 652–660, Jun. 2017.

[12] Yan, S., P. J. Soh, and G. A. E. Vandenbosch, "Dual-band textile MIMO antenna based on substrate-integrated waveguide (SIW) technology," *IEEE Transactions on Antennas and Propagation*, Vol. 63, No. 11, 4640–4647, Nov. 2015.

[13] Ciccia, S., G. Giordanengo, and G. Vecchi, "Energy efficiency in IOT networks: integration of reconfigurable antennas in ultra low-power radio platforms based on system-on-chip," *IEEE Internet of Things Journal*, Vol. 6, No. 4, 6800–6810, Aug. 2019.

[14] Vamseekrishna, A., B. T. P. Madhav, T. Anilkumar, and L. S. S. Reddy, "An IOT controlled octahedron frequency reconfigurable multiband antenna for microwave sensing applications," *IEEE Sensors Letters*, Vol. 3, No. 10, Oct. 2019.

[15] Santamaria, L., F. Ferrero, R. Staraj, and L. Lizzi, "Electronically pattern reconfigurable antenna for IOT applications," *IEEE Open Journal of Antennas and Propagation*, Vol. 2, 546–554, 2021.

[16] Santamaria, L., F. Ferrero, R. Staraj, and L. Lizzi, "Slot-based pattern reconfigurable ESPAR antenna for IOT applications," *IEEE Transactions on Antennas and Propagation*, Vol. 69, No. 7, 3635–3644, Jul. 2021.

[17] Haydhah, S. A., F. Ferrero, L. Lizzi, M. S. Sharawi, and A. Zerguine, "A multifunctional compact pattern reconfigurable antenna with four radiation patterns for sub-GHz IOT applications," *IEEE Open Journal of Antennas and Propagation*, Vol. 2, 613–622, 2021.

[18] Hall, P. S. and Y. Hao, "Antennas and propagation for body-centric wireless communications," *Microwave Journal*, Vol. 55, No. 5, 276, 2012.

[19] Soh, P. J., G. A. E. Vandenbosch, S. L. Ooi, and N. H. M. Rais, "Design of a broadband all-textile slotted PIFA," *IEEE Transactions on Antennas and Propagation*, Vol. 60, No. 1, 379–384, Jan. 2012.

[20] Ullah, M. A., M. T. Islam, T. Alam, and F. B. Ashraf, "Paper-based flexible antenna for wearable telemedicine applications at 2.4 GHz ISM band," *Sensors*, Vol. 18, No. 12, Dec. 2018.

[21] Sharma, S., M. R. Tripathy, and A. K. Sharma, "Low SAR dual-band circularly polarized wearable RFID antenna using FSS reector with reduced EMI," *Progress In Electromagnetics Research C*, Vol. 129, 17–34, 2023.

[22] Sharma, S., M. R. Tripathy, and A. K. Sharma, "Dual-band circularly polarized wearable patch antenna for RFID reader," in *2021 IEEE International Conference on RFID Technology and Applications (RFID-TA)*, 195–198, 2021.

[23] Zhang, J., S. Yan, X. Hu, and G. A. E. Vandenbosch, "Dual-band dual-polarized wearable button array with miniaturized radiator," *IEEE Transactions on Biomedical Circuits and Systems*, Vol. 13, No. 6, 1583–1592, Dec. 2019.

[24] Arif, A., M. Zubair, M. Ali, M. U. Khan, and M. Q. Mehmood, "A compact, low-profile fractal antenna for wearable on-body WBAN applications," *IEEE Antennas and Wireless Propagation Letters*, Vol. 18, No. 5, 981–985, May 2019.

[25] Ashyap, I., S. H. Dahlan, Z. Z. Abidin, H. A. Majid, F. C. Seman, X. Ngu, and N. A. Cholan, "Flexible antenna with his based on PDMS substrate for WBAN applications," in *2018 IEEE International RF and Microwave Conference (RFM 2018)*, 69–72, Penang, Malaysia, Dec. 2018.

[26] Alqadami, A. S. M., K. S. Bialkowski, A. T. Mobashsher, and A. M. Abbosh, "Wearable electromagnetic head imaging system using flexible wideband antenna array based on polymer technology for brain stroke diagnosis," *IEEE Transactions on Biomedical Circuits and Systems*, Vol. 13, No. 1, 124–134, Feb. 2019.

[27] Alqadami, A. S. M., K. S. Bialkowski, A. T. Mobashsher, and A. M. Abbosh, "Wearable electromagnetic head imaging system using flexible wideband antenna array based on polymer technology for brain stroke diagnosis," *IEEE Transactions on Biomedical Circuits and Systems*, Vol. 13, No. 1, 124–134, Feb. 2019.

[28] El Atrash, M., M. A. Abdalla, and H. M. Elhennawy, "A wearable dual-band low profile high gain low SAR antenna AMC-backed for WBAN applications," *IEEE Transactions on Antennas and Propagation*, Vol. 67, No. 10, 6378–6388, 2019.

[29] Can, S. and A. E. Yilmaz, "Reduction of specific absorption rate with artificial magnetic conductors," *International Journal of RF and Microwave Computer-aided Engineering*, Vol. 26, No. 4, 349–354, May 2016.

[30] Hussain, R., "Shared-aperture slot-based sub-6-GHz and mm-wave IOT antenna for 5G applications," *IEEE Internet of Things Journal*, Vol. 8, No. 13, 10 807–10 814, Jul. 2021.

[31] Huang, Y., M. Liu, and Y. Liu, "Energy-efficient SWIPT in IOT distributed antenna systems," *IEEE Internet of Things Journal*, Vol. 5, No. 4, 2646–2656, Aug. 2018.

[32] Sharma, S., M. R. Tripathy, and A. K. Sharma, "Low profile and low SAR flexible wearable patch antenna for WBAN," in *2021 8th International Conference on Signal Processing and Integrated Networks (SPIN)*, 1119–1124, 2021.

[33] Le, T. T. and T.-Y. Yun, "Miniaturization of a dual-band wearable antenna for WBAN applications," *IEEE Antennas and Wireless Propagation Letters*, Vol. 19, No. 8, 1452–1456, Aug. 2020.

[34] Zhang, K., G. A. E. Vandenbosch, and S. Yan, "A novel design approach for compact wearable antennas based on metasurfaces," *IEEE Transactions on Biomedical Circuits and Systems*, Vol. 14, No. 4, 918–927, Aug. 2020.

[35] Gao, G.-P., B. Hu, S.-F. Wang, and C. Yang, "Wearable circular ring slot antenna with EBG structure for wireless body area network," *IEEE Antennas and Wireless Propagation Letters*, Vol. 17, No. 3, 434–437, Mar. 2018.

[36] Seman, F. C., F. Ramadhan, N. S. Ishak, R. Yuwono, Z. Z. Abidin, S. H. Dahlan, S. M. Shah, and I. Ashyap, "Performance evaluation of a star-shaped patch antenna on polyimide film under various bending conditions for wearable applications," *Progress In Electromagnetics Research Letters*, Vol. 85, 125–130, 2019.

[37] Zhang, X. Y., H. Wong, T. Mo, and Y. F. Cao, "Dual-band dual-mode button antenna for on-body and off-body communications," *IEEE Transactions on Biomedical Circuits and Systems*, Vol. 11, No. 4, 933–941, Aug. 2017.

[38] Davoli, L., L. Belli, A. Cilfone, and G. Ferrari, "From micro to macro IOT: challenges and solutions in the integration of IEEE 802.15.4/802.11 and sub-GHz technologies," *IEEE Internet of Things Journal*, Vol. 5, No. 2, SI, 784–793, Apr. 2018.

[39] Cai, Z., Y. Zhou, Y. Qi, W. Zhuang, and L. Deng, "A millimeter wave dual-lens antenna for IOT-based smart parking radar system," *IEEE Internet of Things Journal*, Vol. 8, No. 1, 418–427, Jan. 2021.

[40] Gao, G.-P., C. Yang, B. Hu, R.-F. Zhang, and S.-F. Wang, "A wearable PIFA with an all-textile metasurface for 5 GHz WBAN applications," *IEEE Antennas and Wireless Propagation Letters*, Vol. 18, No. 2, 288–292, Feb. 2019.

[41] Sharma, S., M. R. Tripathy, and A. K. Sharma, "High gain FSS integrated slotted UHF RFID antenna for WBAN," *International Journal of System Assurance Engineering and Management*, Vol. 14, No. SUPPL 2, 2, SI, 610–621, May 2023.

[42] Balanis, C. A., *Antenna Theory: Analysis and Design*, 3rd ed., John Wiley & Sons, 2016.

[43] Munk, B. A., *Frequency Selective Surfaces: Theory and Design*, John Wiley & Sons, New York, 2005.

[44] Ahmed, G., S. U. Islam, M. Shahid, A. Akhunzada, S. Jabbar, M. K. Khan, M. Riaz, and K. Han, "Rigorous analysis and evaluation of specific absorption rate (SAR) for mobile multimedia healthcare," *IEEE Access*, Vol. 6, 29 602–29 610, 2018.

[45] Ansarizadeh, M., A. Ghorbani, and R. A. Abd-Alhameed, "An approach to equivalent circuit modeling of rectangular microstrip antennas," *Progress In Electromagnetics Research B*, Vol. 8, 77–86, 2008.

[46] Kundu, S., "A compact uniplanar ultra-wideband frequency selective surface for antenna gain improvement and ground penetrating radar application," *International Journal of RF and Microwave Computer-aided Engineering*, Vol. 30, No. 10, e22363, 2020.